CHAPTER 3

Equilibrium Studies of Cytochrome Unfolded States

3.1 INTRODUCTION

Proteins are typically denatured *in vitro* in one of three ways: thermally, change in pH, or the addition of organic solutes. Typically the Gray group denatures protein using the chaotropic agents urea and guanidine hydrochloride (GdmCl). Chaotropic agents are organic solutes that induce unfolding by increasing the solubility of nonpolar residues of proteins.[10] Although the mechanism of denaturation using these agents is not completely understood, it is likely that these compounds both solvate the peptide backbone and disrupt hydrogen bonding. It is known that urea and GdmCl differ in some respects: urea has a neutral overall charge and is able to penetrate into hydrophobic areas of proteins, solvating non-polar groups that are usually not exposed to solvents. GdmCl is positively charged, greatly affecting the ionic strength and pH of the solution. It is believed that rather than the penetration seen with urea, GdmCl better disrupts surface interactions of both hydrophobic and hydrophilic residues, resulting in greater solubility of the protein.[11]
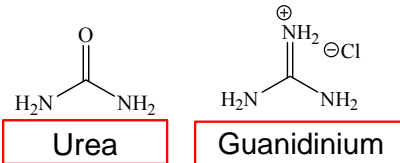
For a given protein, it is well established that the midpoint denaturant concentration (where ½ the population is unfolded and ½ is folded) depends on denaturant properties, and differs substantially for urea and GdmCl. It is also known that protein structure is retained under conditions that, at first glance, should be highly unfolding conditions. For instance, long-range contacts are seen in NMR of staphylococcal nuclease in 9 M urea[7], a common denaturant. Comparison of different denaturing conditions and methods provide insight into the unfolded states of proteins and by extension the folding mechanism and pathways, which is important since folding

rates are assigned assuming a fully extended unfolded state.[5,6] Thermal denaturation is particularly significant since simulations almost exclusively use high temperature to model the unfolding transition. While urea and GdmCl are the most commonly used chemical denaturants for experimental studies, high temperature is the most commonly used *in silico* denaturing technique. This chapter will focus on the effects of these different conditions on heme proteins and the validity of the assumptions regarding the unfolded state.

3.2 RESULTS AND DISCUSSION

3.2.2 Steady-State Equilibrium Unfolded States of Iron and Zinc-Substituted Heme Proteins

In conjunction with the isotope and bimolecular quenching experiments in Chapter 2, the unfolding midpoints were measured for Zn-cyt *c*. As seen in Figure 3.1, the midpoints in GdmCl and urea were determined to be 3.2 M and 6.9 M, respectively. The implication from these thermodynamic experiments is that GdmCl unfolds Zn-cyt *c* more effectively when compared with urea. However, the free energies of unfolding calculated from the titration curve were found to be similar (ΔG_f° = -31 kJ/mol for urea and ΔG_f° = -34 kJ/mol for GdmCl). This provides some evidence that the two chemicals, though very different in their mechanism of action, unfold the protein to the same, fully extended state. It is of note that the zinc-substituted protein and Fe(III)-cyt *c* have very similar midpoints in GdmCl, as illustrated in Figure 3.2.

While the chemically-induced unfolded states are similar for Zn-cyt *c* in the UV-Vis and CD steady-state techniques, the protein conformation is noticeably different at elevated temperature (Figure 3.3). The CD temperature titration (Figures 3.4)
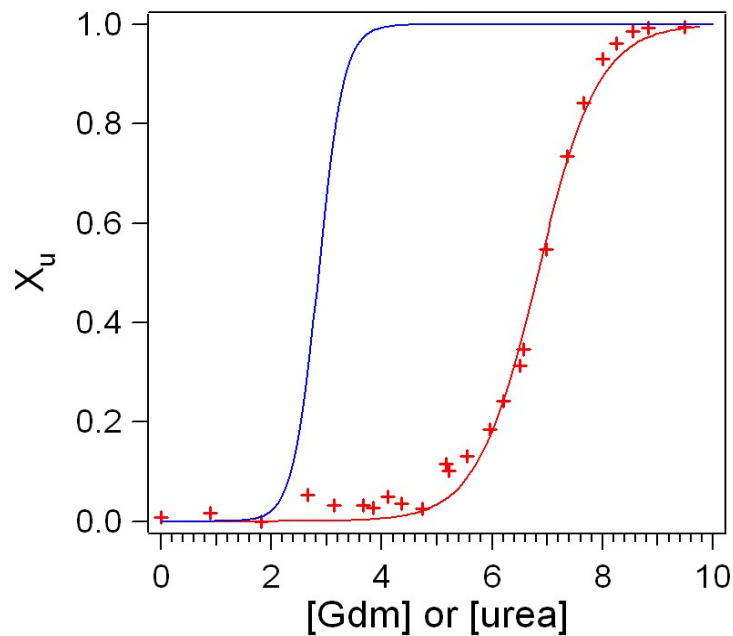
Figure 3.1. Equilibrium unfolding curves of Zn-cyt *c* in GdmCl (blue) and urea (red). The GdmCl data was adapted from the thesis of Jennifer Lee.
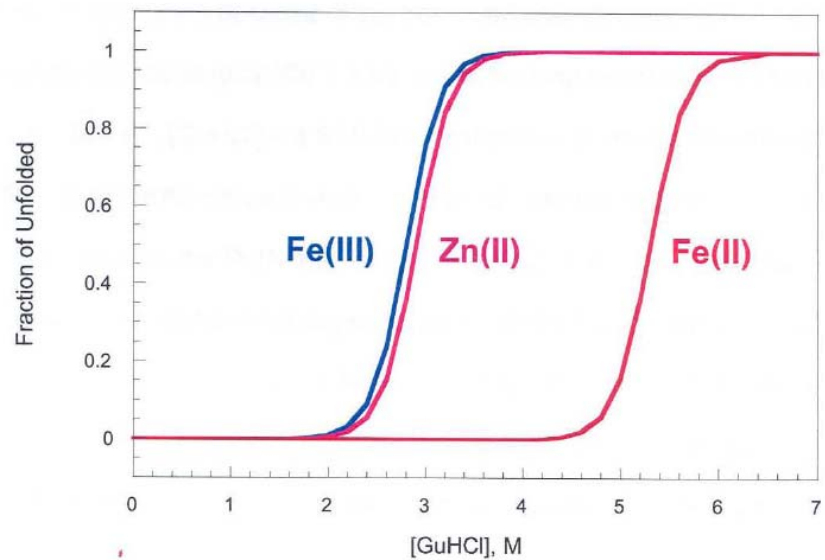

Figure 3.2. Equilibrium unfolding curves of iron and zinc-substituted cyt *c*. Adapted from the thesis of Jennifer Lee.

illustrates that Zn-cyt *c* does lose alpha-helical structure as temperature increases; however, it never reaches the extended structure that is characteristic of the protein in 6 M GdmCl or 9 M urea. UV-Vis spectroscopy also demonstrates the difference in behavior of Zn-cyt *c* in GdmCl and at elevated temperature. In 5 M GdmCl, the λ_{max} of the Zn-cyt *c* Soret band blue shifts from the 423 nm maximum of the folded state to 418 nm. A temperature titration of Zn-cyt *c* reveals no blue-shift, but rather a nearly 8-fold increase in molar absorptivity (Figure 3.3). Fe-cyt *c* and both Fe- and Zn-cyt *c'* also do not exhibit a blue-shift, however their molar absorptivities only increase by ~1.05, 1.3, and 1.75, respectively.

The more hydrophobic four-helix bundle proteins Zn-cytochrome *c'* and Zn-cytochrome cb_{562} exhibit even less evidence by circular dichroism of losing alpha-helical structure at elevated temperature than Zn-cyt *c* (Figure 3.6). In these cases, the transition is not cooperative and the signal does not appear to level off, even at the highest temperatures, indicating that the protein never reaches an equilibrium extended structure. For Zn-cyt *c*, *c'* and cb_{562}, this behavior deviates from the Fe-porphyrin of the native proteins, which shows more cooperative transitions and lower midpoint temperatures, but certainly the greatest difference is seen between chemical denaturation and temperature denaturation.

The emission of the native tryptophan is quenched by the heme absorbance in the folded states of both Fe- and Zn-cyt *c*. Since the fluorescence intensity is related to the distance between the tryptophan donor and the heme acceptor, it is seen in Figures 3.9 and 3.10 that the most extended structures are seen for GdmCl, followed by urea. For Zn-cyt *c*, the fluorescence intensity at elevated temperatures is even less than that for the
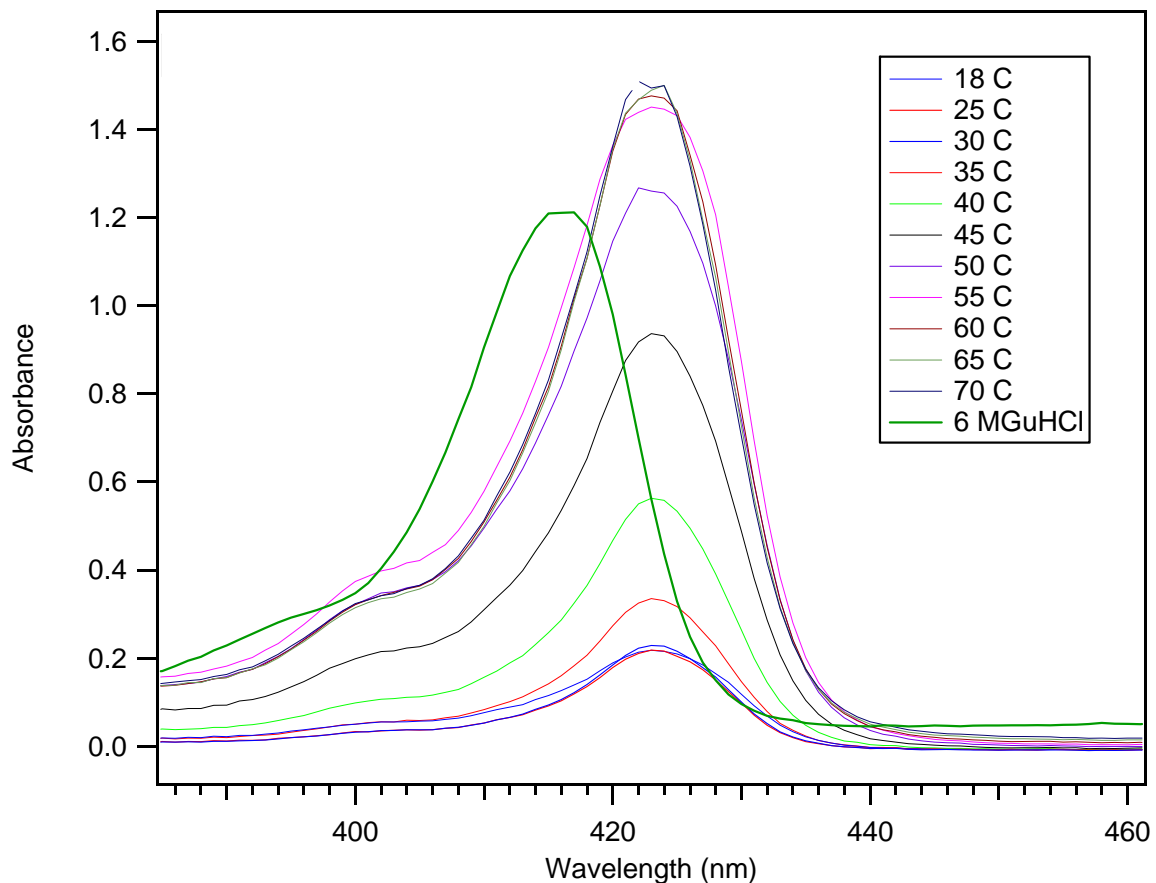
Figure 3.3. UV-Vis Spectra of Zn-cyt *c* in 6 M GdmCl (dark green) and for various temperatures ranging from 18 °C to 70 °C in 20 mM NaPi, pH 7.0. The temperature spectra were collected from the same protein sample.
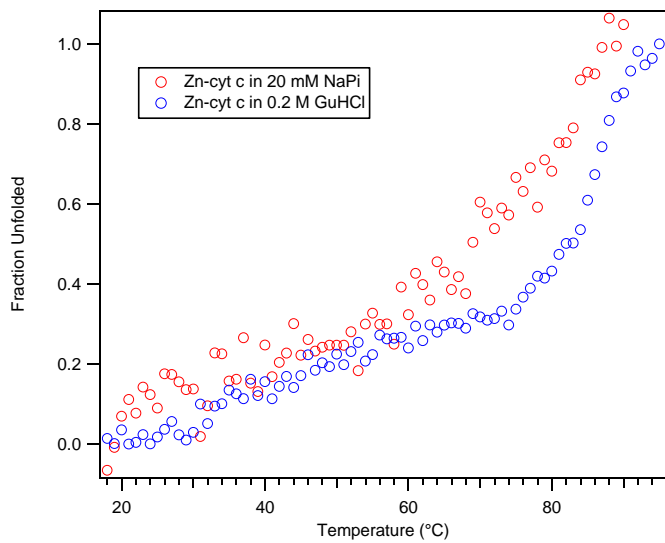
Figure 3.4. CD temperature unfolding curve Zn-cyt *c* in 20 mM NaPi (red) and 200 mM GdmCl (blue).
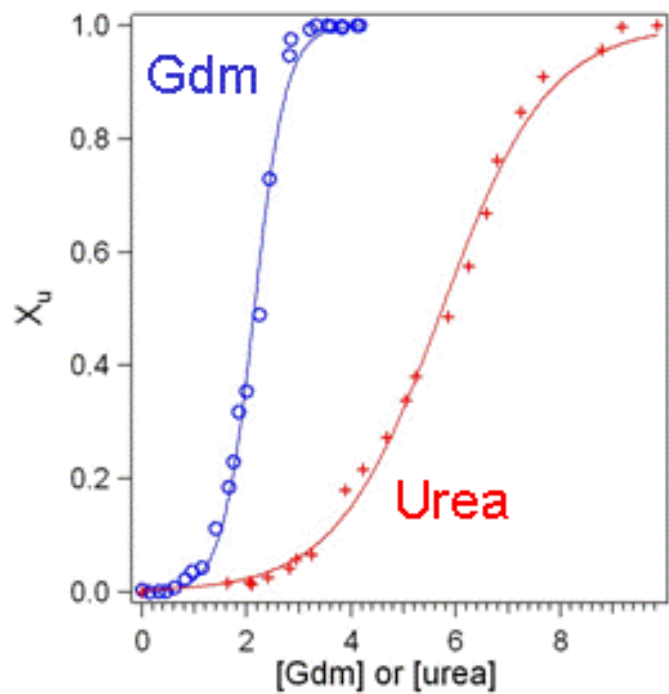

Figure 3.5. Equilibrium unfolding curves of Zn-cyt *c'* in GdmCl (blue) and urea (red).
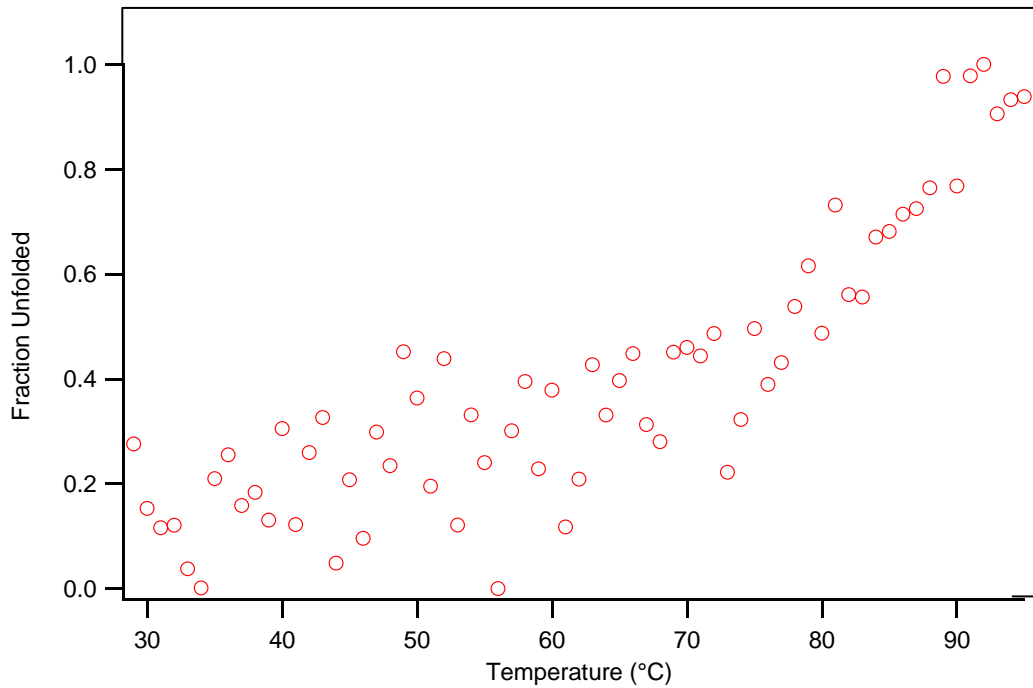
Figure 3.6. CD temperature unfolding curve of Zn-cyt cb_{562}.
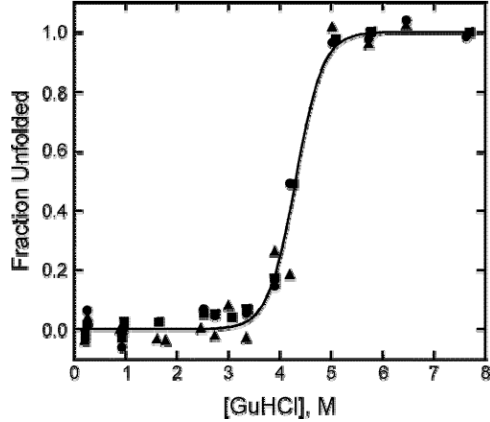
Figure 3.7. GdmCl unfolding curve of Fe-cyt cb_{562}, adapted from data from Jasmin.
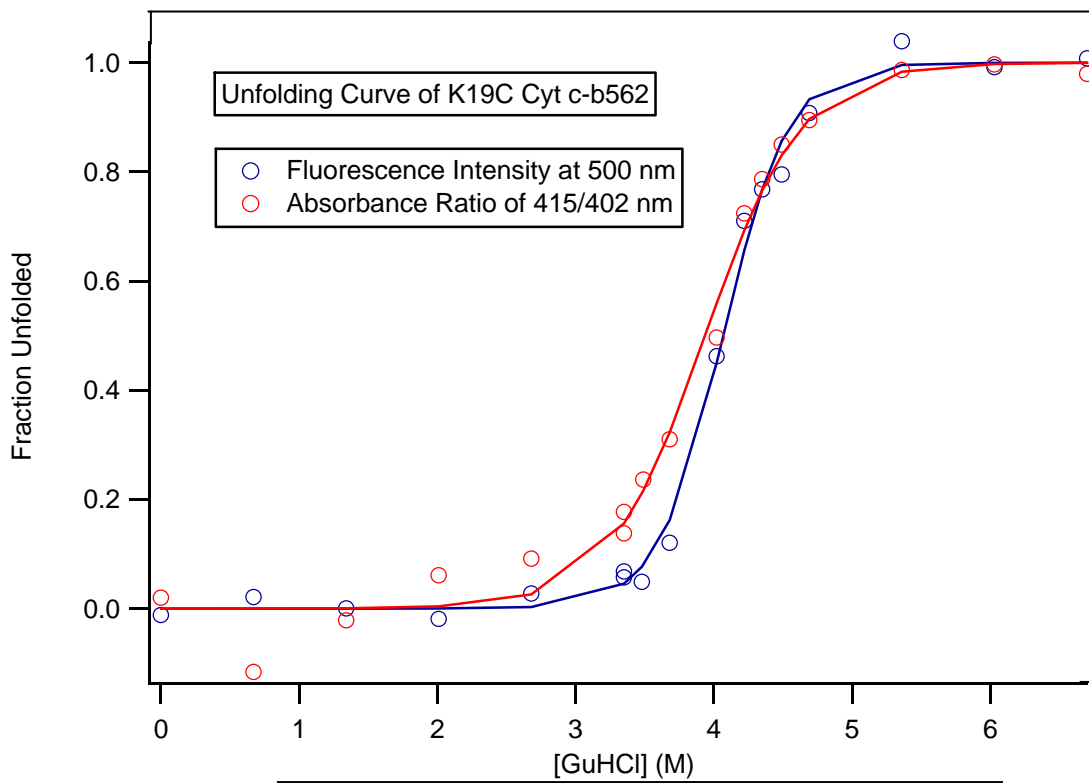
Figure 3.8. GdmCl unfolding curve of DNS(K19C)-cyt cb_{562} monitored by steady-state fluorescence emission at 500 nm and by the absorption (415/402). Protein concentration is 1uM in 50 mM NaOAc pH 5.
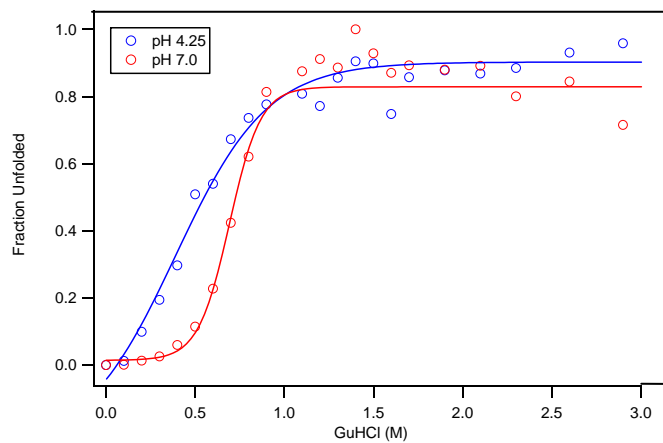
Figure 3.9. GuHCl unfolding curve of DNS(C102)-cyt c at pH 4.25 (blue) and pH 7 (red), monitored by steady state fluorescence emission.
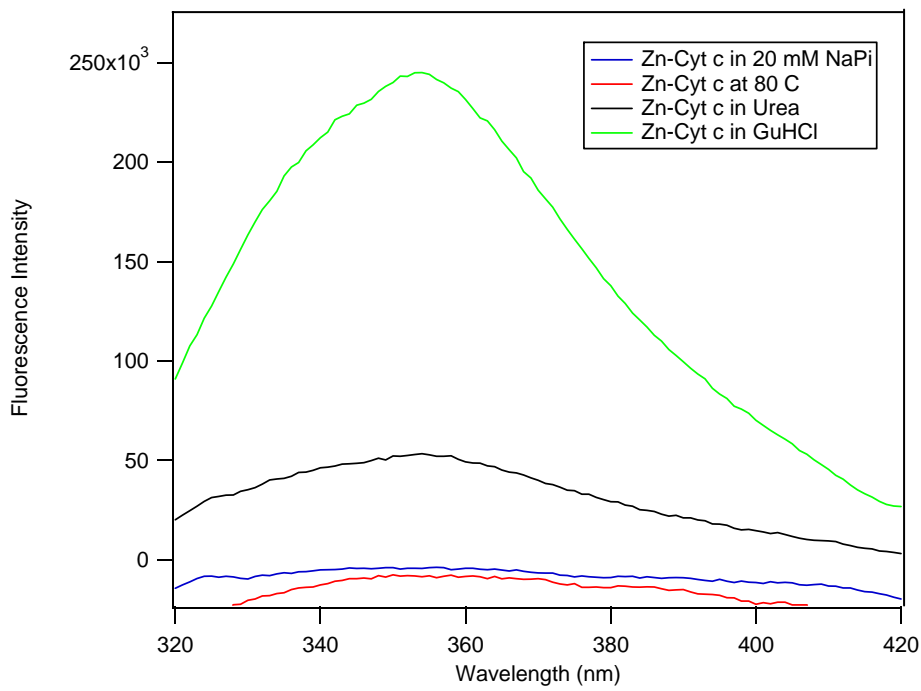
Figure 3.10. Steady state fluorescence spectra of Zn-cyt *c* in 6 M GdmCl (green), 7 M urea (black), 20 mM NaPi (blue) and in buffer at 80 °C (red). All spectra were background subtracted.
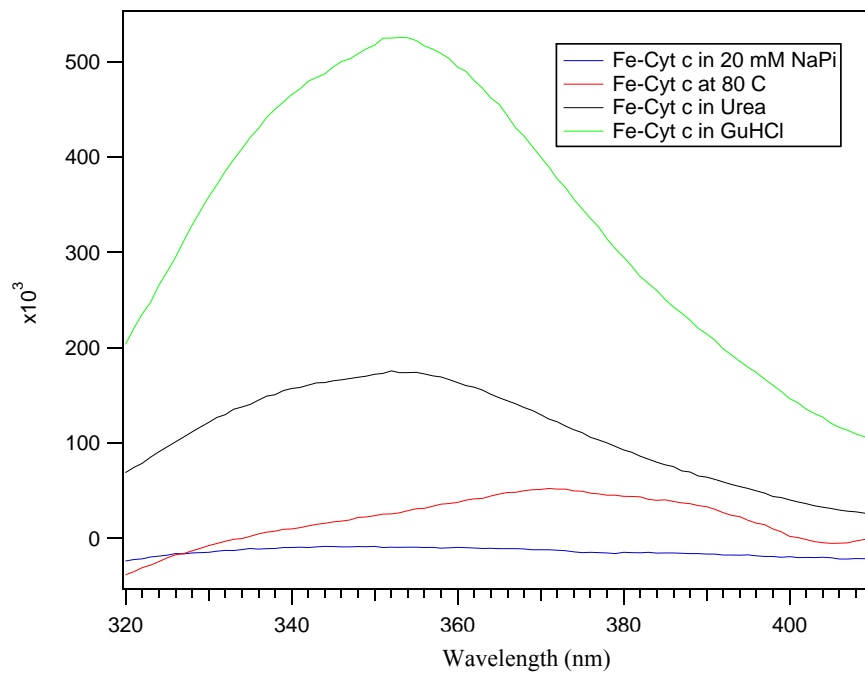
Figure 3.11. Steady state fluorescence spectra of Fe-cyt *c* in 6 M GdmCl (green), 7 M urea (black), 20 mM NaPi (blue) and in buffer at 80 °C (red). All spectra were background subtracted.
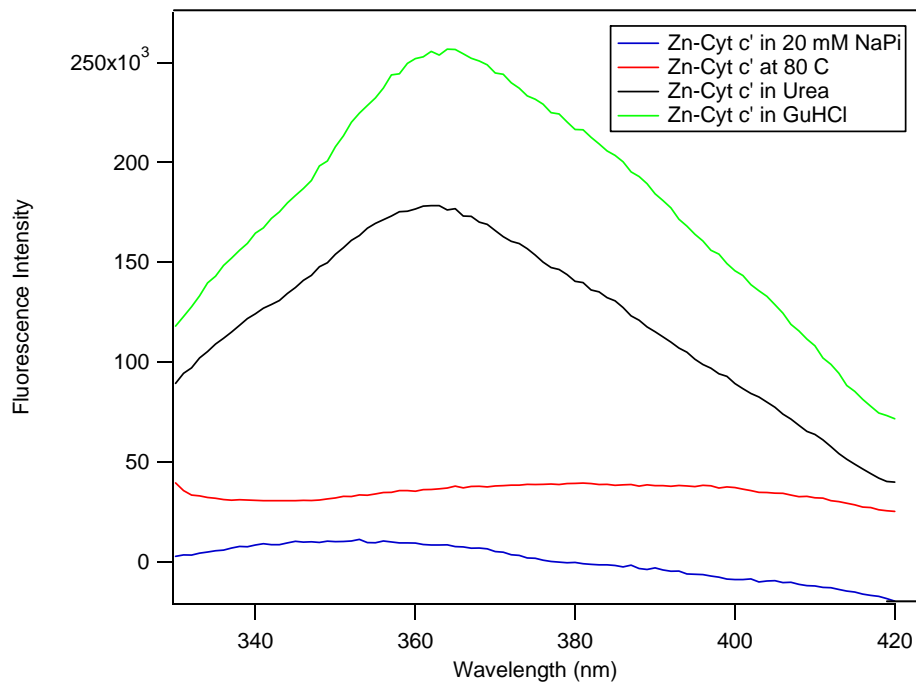
Figure 3.12. Steady state fluorescence spectra of Zn-cyt *c'* in 6 M GdmCl (green), 7 M urea (black), 20 mM NaPi (blue) and in buffer at 80 °C (red). All spectra were background subtracted.
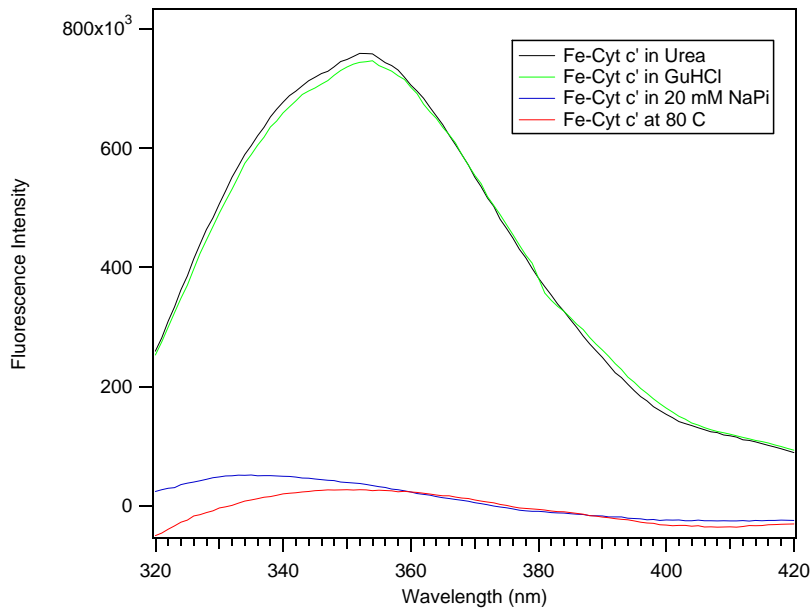
Figure 3.13. Steady state fluorescence spectra of Fe-cyt *c'* in 6 M GdmCl (green), 7 M urea (black), 20 mM NaPi (blue) and in buffer at 80 °C (red). All spectra were background subtracted.

folded protein. Rather than forming a more compact structure, which would result in greater fluorescence quenching, it is likely that the greater absorbance seen at elevated temperatures changes the overlap integral of the **D-A** pair. The FET kinetics of the W-heme **D-A** pair are needed to confirm this conclusion. While this phenomenon is not seen for Fe-cyt *c*, Zn-cyt *c'* or Fe-cyt *c'*, the trend of greater extended conformation in GdmCl, then urea, then elevated temperature continues (Figures 3.10, 3.11, and 3.12).

3.2.4 Transient Absorbance Experiments of Denatured States

Transient absorbance measurements were performed on Zn-cyt *c* in GdmCl and urea in order to gain insight into microenvironment differences (Figure 3.14). When the lifetimes of the triplet excited state in fully unfolded protein (~5 M GdmCl and ~8 M urea) were investigated in the two different denaturants it was found that the rate of decay was faster in GdmCl. This trend was also true for Zn-MP8, with a triplet state lifetime approximately three times longer in urea than in GdmCl. It is possible that this difference is attributable to the much higher ionic strength of the GdmCl solutions. An interesting result from the experiments in these denaturants is that the triplet

	k_{H2O} (s^{-1})	k_{D2O} (s^{-1})	k_{H2O}/k_{D2O}
ZnAcMP8 in phosphate	3030	1990	1.5
guanidine	6980	4955	1.4
urea	2325	1580	1.5
Zn-cyt *c* in phosphate	105	90	1.2
guanidine	810	600	1.4
urea	720	525	1.4

Table 3.1. Rate constants and isotope effects for ZnAcMP8 and Zn-cyt *c* Triplet States.

lifetimes of ZnAcMP8 remain much shorter when compared to Zn-cyt *c* (3-9 times faster), indicating that the heme is still partially protected even under fully unfolded conditions. Since the vibrational spectra of the two denaturants are similar in the high
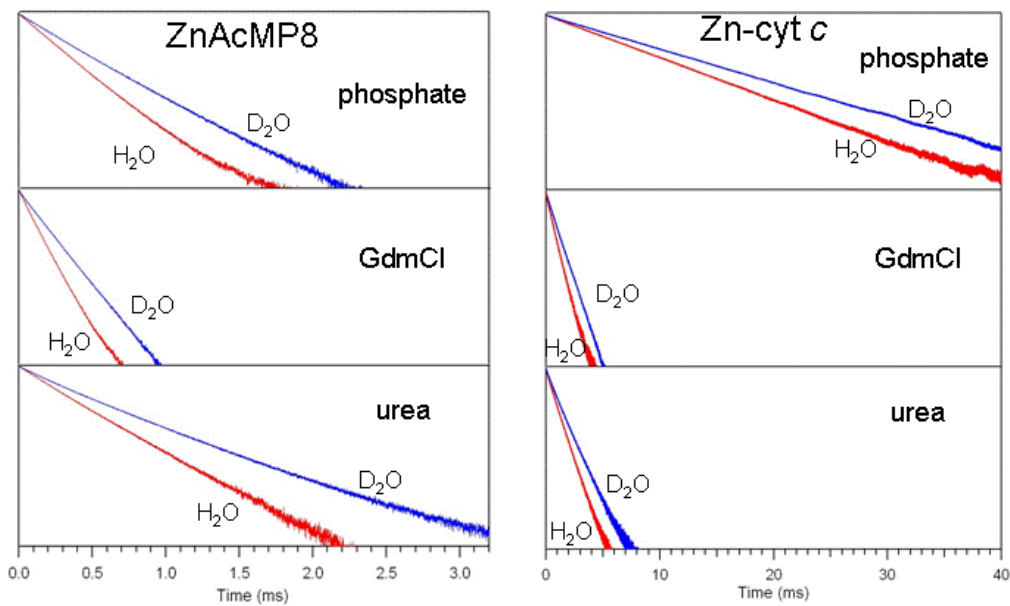
Figure 3.14. Transient absorption decay kinetics of triplet ZnAcMP8 (left) and Zn-cyt *c* (right) in protonated and deuterated solutions. Buffers were 20 mM phosphate (top) with ~5 M GdmCl (center) or ~9 M urea (bottom).
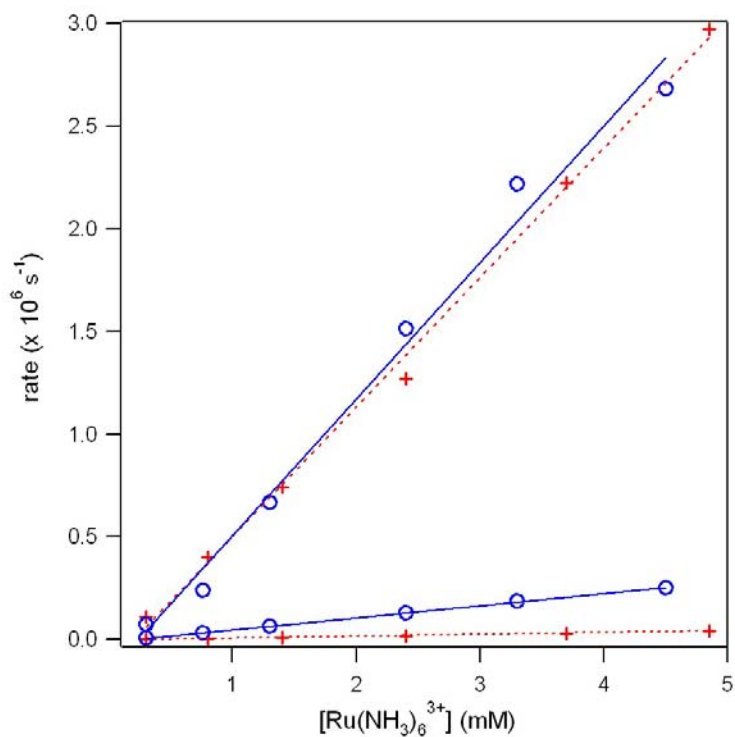
Figure 3.15. Rate constants from fast and slow components of transient absorption decay kinetics of triplet Zn-cyt *c* at the midpoint in GdmCl (blue) and urea (red) solutions at various concentrations of $Ru(NH3)_6^{3+}$ quencher.
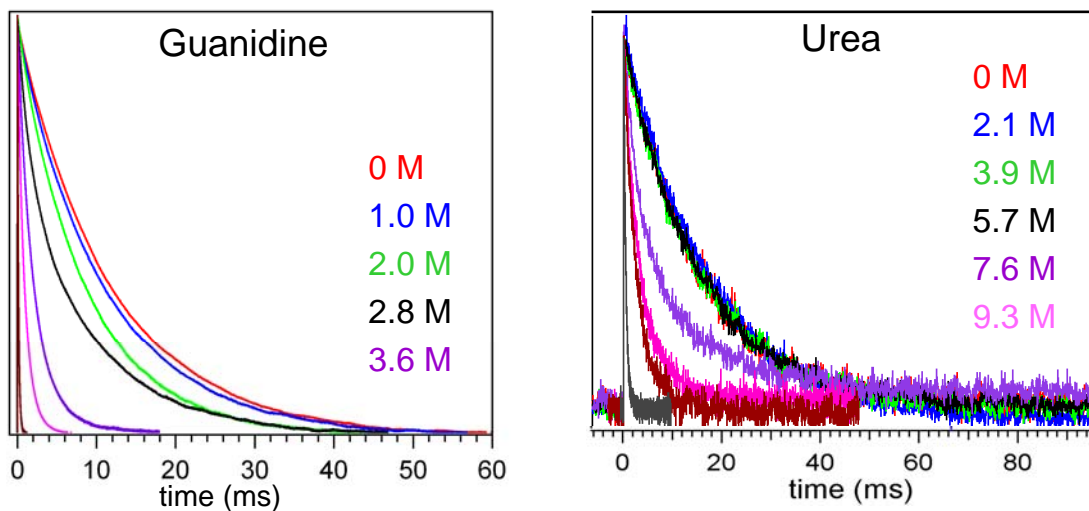
Figure 3.16. Transient absorption decays of triplet Zn-cyt *c* at various GdmCl (left) and urea (right) concentrations.
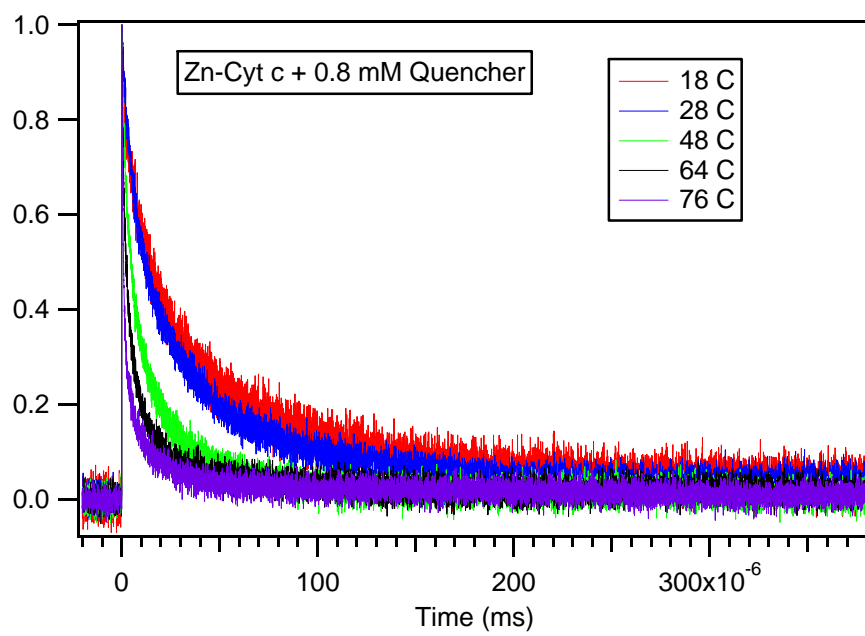
Figure 3.17. Transient absorption decays of triplet Zn-cyt *c* with 0.8 mM Ru(NH$_3$)$_6$ at various temperatures ranging from 18 $^{\circ}$C to 76 $^{\circ}$C.

frequency region, the difference in decay rates may reflect the role of ionic strength in triplet deactivation for the fully exposed Zn-porphyrin.

For the fully unfolded protein, triplet decays increase 500-800 times upon addition of quencher from pure decay rates of 810 (GdmCl) and 720 (urea) s^{-1} to 4.4–6.4 x 10^5 and 4.8 x 10^5 s^{-1}, respectively. This increase in quenching rate is primarily due to greater porphyrin accessibility to the quencher in the unfolded protein, and may also reflect the change in ionic strength in the GdmCl case.[21] Rate constants at denaturant midpoints are displayed in Figure 7, along with linear fits. The second-order rate constants are 6.6 x 10^8 (extended) and 5.9 x 10^7 (compact) M^{-1} s^{-1} in GdmCl, and 6.3 x 10^8 (extended) and 8.6 x 10^6 (compact) M^{-1} s^{-1} in urea. These rate constants are similar to those obtained in our previous work.[23] The change in lifetime cannot be attributed solely to the change in heme-solvent vibronic coupling in water relative to denaturant; our studies with ZnAcMP8 indicate that a change in cosolvent affects triplet lifetimes only by a factor of ~3. Instead, the decreased lifetime reflects enhanced Zn-porphyrin solvation, and this interpretation is further supported by the larger isotope effect and greater quencher accessibility for unfolded relative to folded protein. The variation in Zn-porphyrin solvation for the compact states in the two denaturants reveals that the cofactor in the partially unfolded protein is better protected in urea solutions.

A molecular description of the mechanism of chemical denaturation is a goal of much current research.[10] For Zn-cyt c, the free energies of unfolding are comparable in urea (ΔG_f^o = -31 kJ/mol) and GdmCl (ΔG_f^o = -35 kJ/mol), and the difference in midpoints may be attributable to ionic strength effects.[15] In addition, fully unfolded proteins in high urea and GdmCl concentrations exhibit similar triplet lifetimes, isotope effects, and

bimolecular quenching rates, suggesting that these denaturants create nearly identical

localized heme environments under these conditions. Unfolded extended structures

formed at midpoint urea and GdmCl concentrations also exhibit indistinguishable solvent

accessibility, demonstrated by similarly high second-order rate

constants. Our observation that these triplet quenching rates for fully unfolded protein in

the two denaturants are virtually identical suggests that ionic strength plays a minor role

in bimolecular quenching of unfolded relative to folded[25] Zn-cyt *c*.

In contrast to fully denatured protein, the structure of the compact species

depends on denaturant. Bimolecular quenching of the triplet Zn-porphyrin in the compact

state in urea is ~ 7 times slower than in GdmCl, and this difference likely reflects greater

protection of the porphyrin group from the aqueous urea solvent. An additional

contribution to this difference may come from electrostatic effects, since it has been

shown that bimolecular quenching of the protected cofactor in folded Zn-cyt *c* is sensitive

to ionic strength and quencher charge.[35] However, the bimolecular quenching rates

observed here are similar to those reported for folded and molten globule states of Zn-cyt *c*,[25] supporting our interpretation that the rate

Gdm	urea
Fast: 6.6×10^8 s^{-1} M^{-1}	Fast: 6.3×10^8 s^{-1} M^{-1}
Slow: 5.9×10^7 s-1 M-1	Slow: 8.6×10^8 s-1 M-1

Table 3.2. Rate constants of fast and slow components of Zn-cyt *c* triplet state decays in the presence of 0.8 M quencher at the midpoint concentration of denaturant.

differences are attributable to variations in the equilibrium GdmCl- and urea-induced

compact structures. It is possible that these partially unfolded species are similar to the

intermediates associated with the burst phase (hydrophobic collapse) of cytochrome *c*

folding.[12,14,23,26] The compact structure observed here likely represents this partially

unfolded intermediate as well, and our finding that the structure of this species is denaturant-dependent supports the notion of nonnative cofactor environments for this compact, partially unfolded species.

The bimolecular quenching of Zn-cyt *c* at elevated temperatures follows the trend seen for the chemical denaturants urea and GdmCl (Figure 3.15). The greatest quenching is seen for the highest temperature of 75 °C, indicating that the the protein is most extended and the porphyrin is most solvent exposed at this temperature.

3.2.5 Fluorescence Energy Transfer Under Different Denaturing Conditions

The proposal that urea creates a more compact species than GuCl is supported by fluorescence energy transfer kinetics experiments on Zn-cyt *c* (Figure 3.18). Based on the FET lifetimes, the average distance between Trp59 and the Zn-porphyrin is shorter at high urea concentrations than in GdmCl. This extra compaction in urea may reflect the relative strengths of these two widely-used denaturants.

unfolded folded

Fluo of Trp59
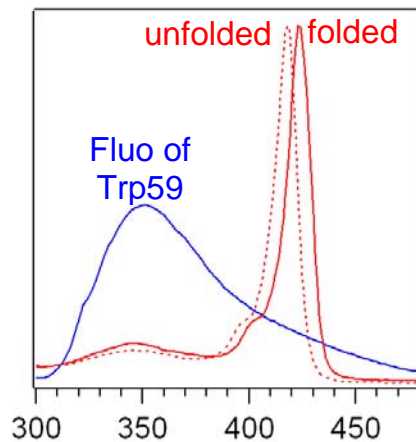
$\Phi_{fl} \sim$ 0.13 in H2O
           0.15 in Guanidine
           0.23 in Urea

$R_0 =$ 29 Å for trp-heme
         $9 < r < 44$

Rate constants

Distances

buffer

urea

guanidine

amplitude

buffer

urea

guanidine

k (ns^{-1})

r (Å)
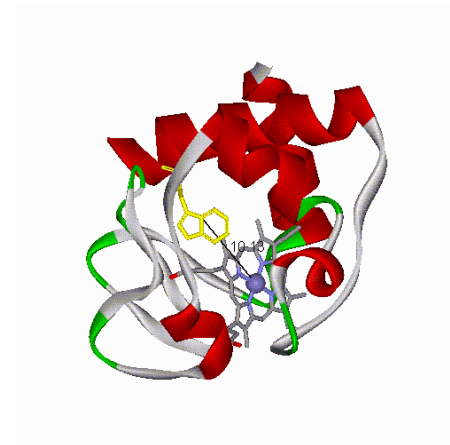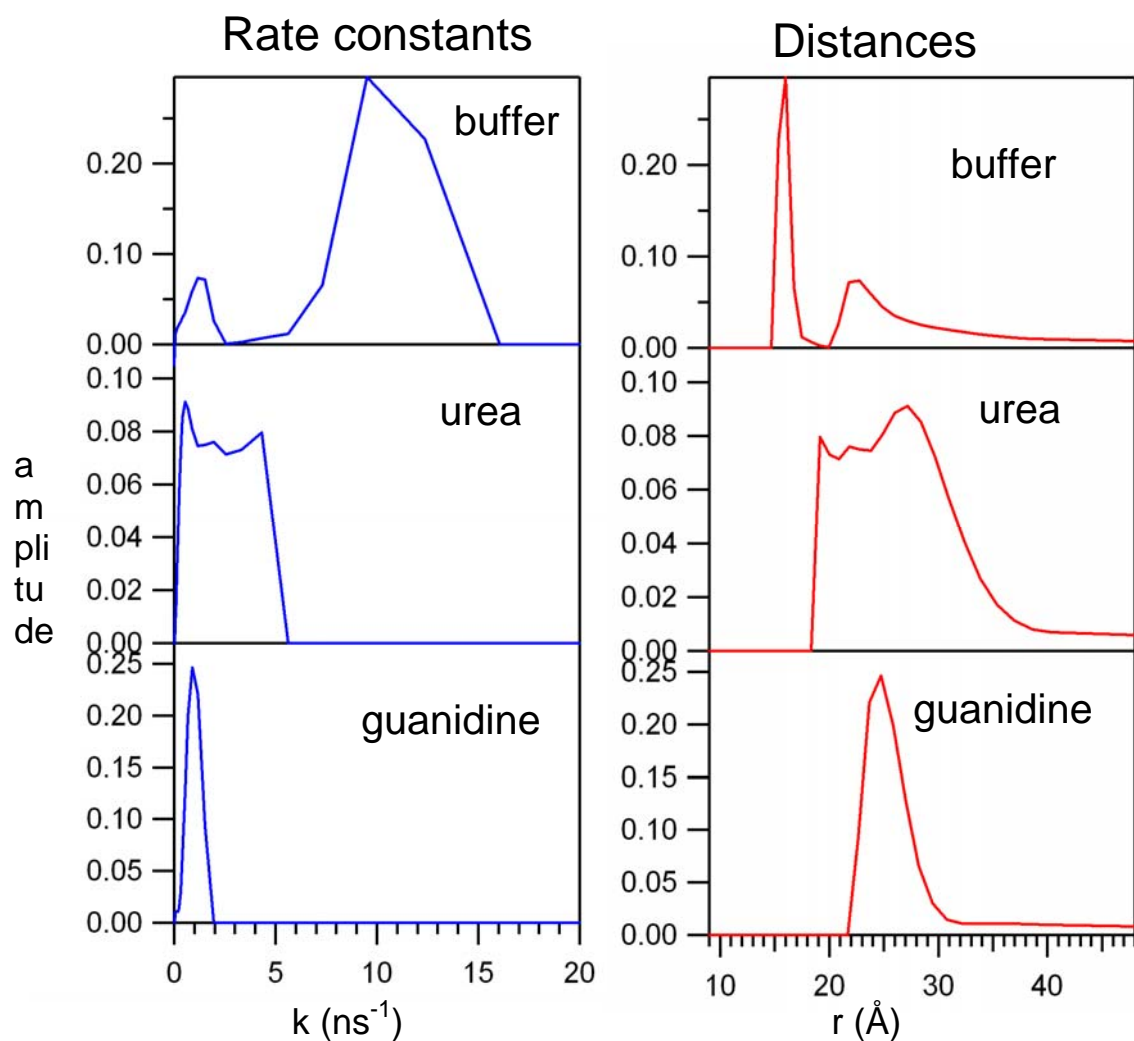
Figure 3.18. Distributions from maximum entropy analysis of fluorescence decay rates (P(k), left) and **D-A** distances (P(r), right) for Zn-cyt c in 20 mM NaPi (top), urea (middle), and GdmCl (bottom).

3.3 CONCLUSIONS

There is general consensus that chemical denaturants act through a combination of direct binding to the peptide backbone and residues, and by altering the hydrogen bonding network of water in a structure-making or structure-breaking manner, thereby diminishing the hydrophobic effect.[9,10] It is well established that the transfer free energy for the peptide group from water to aqueous solutions of urea or GdmCl is favorable, with GdmCl being a better solvent for the peptide backbone than urea.[17] In contrast, side chains show wide variability in transfer free energy to denaturant solutions; however, for a given denaturant concentration, GdmCl is more effective in its ability to solvate both hydrophobic and hydrophilic residues.[18,19] Studies on charge effects suggest, not surprisingly, that denaturation by urea is more sensitive to protein charge and ionic strength than GdmCl.[13-15,20] Collectively, these reports indicate that GdmCl is more effective than urea in its ability to disrupt and solvate hydrophobic pockets of folded proteins, in agreement with our finding that the Zn-porphyrin in the compact state of Zn-cyt *c* is more exposed to solvent in GdmCl than in urea.

3.4 METHODS AND MATERIALS

3.4.2 Protein Preparation

Zn-cyt *c* and ZnAcMP8 were prepared as described in Chapter 2.

Q1A cyt *c'* was expressed following the protocol outlined in the thesis of Jennifer C. Lee. The plasmid was co-transformed with pEC86 into BL21 competent cells following standard transformation protocols. An empty DNA tube (Falcon 35-2059) was placed on ice for 30 minutes. 50 µL of competent cells were added to the cold tube, which was immediately placed back on ice. 1 µL of the DNA was added to the tube,

which was tapped 2-3 times and immediately placed back on ice where it remained for 5 minutes. The DNA tube was then placed in 42 °C water bath for 60 seconds and then placed on ice for two minutes. 200 μL of warm (37 °C) NZY broth was added to the DNA solution. The tube was placed in the 37 °C shaker for 1 hour, after which it was plated on fresh, dry plates under sterile conditions. Single colonies were selected and used to inoculate DNA tubes containing 3 mL LB, 100 μg/mL ampicillin and 30 μg/mL of chloramphenicol. After growing overnight, the DNA tubes were spun down and the cell pellet with the brightest red color was selected for further growth. At this point, frozen glycerol stocks were prepared and frozen in the -80 °C freezer.

Large scale protein expression is optimized by first growing pre-cultures overnight. These cultures are spun down and the resulting red-colored cell pellets were rinsed with fresh media and then used to inoculate 1 to 1.5 liters of media. After 16-20 hours of growth, the cells were harvested via centrifugation and kept on ice. The cell pellet was resuspended in a sucrose solution of 20% sucrose, 1 mM EDTA and 30 mM Tris, pH 8. The cells visibly swell at this point. The suspension was centrifuged at 5000 rpm for 5–10 min. The resulting pellets were then resuspended in a cold 5 mM MgSO$_4$ solution, and this suspension was centrifuged at 8500 rpm for 40–60 min. The supernatant was collected and treated with a protease inhibitor (1 mM PMSF).

Prior to column chromatography, the crude protein extract was diluted with cold water to an ionic strength of 5 mM; and the pH was adjusted to 5.0 with concentrated acetic acid. This solution was loaded on a Fast Flow CM Sepharose column equilibrated with 5 mM NaOAc buffer at pH 5.0. The column was washed with 5 mM NaOAc buffer at pH 5.0 and the protein was eluted with a stepwise salt gradient (0–0.25 M NaCl). The

eluted protein was concentrated, and the solution exchanged to 5 mM MES, pH 5.5 either by dialysis or repeated ultrafiltration. The protein was further purified by ion-exchange chromatography with a Mono S or HP SP Sepharose column using an FPLC system (Pharmacia). The column was equilibrated with 5 mM MES buffer at pH 5.5 and the protein was eluted with a linear salt gradient from 0 to 0.2 M NaCl in 5 mM MES buffer at pH 5.5. The protein purity was judged by the 0.19–0.21 $A_{280}:A_{398}$ ratio and also checked with SDS gel electrophoresis and electrospray mass spectrometry. The protein concentration was determined from the known absorptivity ε_{398} of 89 mM^{-1} cm^{-1}.
E. coli cyt *cb* $_{562}$ was expressed by cotransforming the construct pETcb562 with pEC86 into *E. coli* strain BL21 (DE3). Cyt *c-b* $_{562}$ was purified by ion exchange chromatography on CM Sepharose Fast Flow and followed by a second purification step on a Mono S column (FPLC, Amersham Pharmacia). Proteins were judged to be pure by SDS/PAGE (PhastSystem, Amersham Pharmacia) and electrospray ionization-MS analysis (Caltech Protein/Peptide Microanalytical Laboratory).

The zinc substitution of cyt *c'* and cyt *cb*$_{562}$ was similar to that described in Chapter 2 for cyt *c*. Zn(II) incorporation was monitored via the Soret red-shift from the free base to Zn-porphyrin. Crude protein was washed by dialysis into 20 mM potassium phosphate buffer (pH 7.0), loaded onto a cation exchange column (HiTrap CM, Amersham Biosciences) and eluted using a linear gradient up to 0.5 M NaCl. The excess zinc and salts were removed via dialysis into 20 mM potassium phosphate buffer (pH 7.0) and the protein was further purified by FPLC (HiTrap CM cation exchange column, Amersham Biosciences) and eluted with a linear gradient to 0.5 M NaCl.

3.4.3 Steady-state Equilibrium Experiments

Absorption spectra were recorded on a Hewlett-Packard 8453 diode-array spectrophotometer (Santa Clara, CA). Protein concentrations were estimated by using ε_{410} = 243 000 M^{-1} cm^{-1} for Zn-cyt *c*. Circular dichroism data were acquired using an Aviv Model 62ADS spectropolarimeter (Aviv Associates, Lakewood, NJ) equipped with a thermostated sample holder. Scans were recorded from 210 to 260 nm at 1-nm intervals with an integration time of 5 s and a bandwidth of 1.5 nm. Spectra were collected at 20° C and in a 1-mm fused-silica cuvette unless otherwise specified. The thermal unfolding curve was generated from the ellipticity at 222 nm, recorded from 20 °C to 80 °C at 1 °C intervals. All spectra were background subtracted.

Steady-state fluorescence measurements were performed with a Jobin Yvon/SPEX Fluorolog spectrofluorometer (HORIBA Jobin Yvon, Model FL3-11, Edison, NJ) equipped with a Hamamatsu R928 PMT (Hamamatsu Photonics, Bridgewater, NJ). Samples (~1 μM) were excited at 290 nm (2-nm band-pass) and luminescence was observed from 420 to 650 nm at 1-nm intervals with 0.5 s integration times at room temperature or as otherwise specified. Background spectra of buffer only were also recorded and subtracted from cyt *c* spectra.

3.4.4 Transient Absorption Experiments

We have measured transient absorption spectra of the Zn-porphyrin triplet in ZnAcMP8 and Zn-cyt *c*; the change in absorbance from 420-500 nm due to formation of triplet state in ZnAcMP8 is displayed in Figure 2.1 along with the ground-state absorption spectrum. Our work shows that triplet ZnAcMP8 exhibits an absorption maximum near 440 nm, whereas triplet Zn-cyt *c* absorbs strongly near 460 nm, consistent with previous results.[34,39] Comparison with the ground-state Zn-cyt *c* bleach reveals an

increase in molar extinction coefficient of 30-40 mM^{-1} cm^{-1} at 450 nm upon formation of triplet Zn-cyt *c*. Thus, 450 nm is an excellent probe wavelength for the Zn-porphyrin triplet state, since ground-state absorption, cation radical absorption (λ_{max} ~675 nm),[34] and triplet luminescence (λ_{max} ~736 nm) are minimal at this wavelength.[34,40]

A 10 Hz, 10 ns Nd:YAG laser with a 355 nm-pumped optical parametric oscillator was used to form the transient triplet state of Zn-porphyrin. The probe was a continuous-wave 75 W xenon arc lamp. The 550 nm, 1.6-mm diameter pump and 450 nm, 0.7-mm diameter probe beams were collinear in a 1-cm quartz cuvette. Signal light was dispersed in a 10-cm, F/3.5 double monochromator (DH10, Instruments, S.A.) and detected by a PMT. Power dependence experiments verified that under these conditions, pump (1.0-1.5 mW) and probe (1.8-2.3 mW) powers were well within the linear regime for triplet formation and decay. Reported kinetics curves are the average of 1000 shots, and photodegradation of the degassed 1-4 μM Zn-cyt *c* solutions (20 mM phosphate, pH=pD=7.4) monitored by UV/vis absorption spectroscopy was typically <10% after each experiment. For ZnAcMP8 (2-3 μM in 20 mM phosphate + 0.1% TFA) bimolecular quenching experiments with Ru(NH$_3$)$_6$$^{3+}$, no photodegradation was detected.

3.4.5 Fluorescence Energy Transfer Kinetics

Fluorescence decay measurements were performed using the third harmonic of a regeneratively amplified Nd-YAG laser (355 nm, 50 ps, <0.5 mJ) for fluorophore excitation and a picosecond streak camera (Hamamatsu C5680) in photon counting mode for detection. Magic-angle polarization was used for both excitation and collection. DNS fluorescence was selected with a 420-nm long-pass cutoff filter.

The third harmonic of a femtosecond Ti:Sapphire regenerative amplifier (Spectra-Physics) was used to excite tryptophan at a 1kHz repetition rate with 292 nm light. The time resolution of the laser, determined by the full width at half maximum (FWHM) of the instrument response function, is 300 ps. Excitation power at the sample was ~550-650 µW and a 355 ± 5nm (or 325 ± 5nm) filter was used to select for tryptophan emission. A UG11 glass filter was used that allows passage of only ultravisible light below 400nm. Emission was transferred using an optical fiber connected to a picosecond streak camera (Hamamatsu C5680) in photon-counting mode. Measurements were recorded under magic angle polarization conditions (O'Connor & Phillips, 1984) and emission was detected at 90° to the excitation beam. Minimal photobleaching (< 10%) was confirmed by recording UV-visible absorption spectra before and after laser measurements.

REFERENCES

(1) Dunbar, J.; Yennawar, H. P.; Banerjee, S.; Luo, J.; Farber, G. K. The Effect of Denaturants on Protein Structure. *Protein Science* **1997,** 6, 1727-1733.

(2) Vanzi, F.; Madan, B.; Sharp, K.Effect of the Protein Denaturants Urea and Guanidinium on Water Structure: A Structural and Thermodynamic Study. *J. Am. Chem. Soc.* **1998,** 120, 10748-10753.

(3) Sudha, B. P.; Dixit, S. N.; Moy, V. T.; Vanderkooi, J. M. Reaction of Excited-state Cytochrome *c* Derivatives- Delayed Fluorescence and Phosphorescence of Zinc, Tin, and Metal-free Cytochrome *c* at Room Temperature. *Biochemistry* **1984,** 23, 2103-2107.

(4) Caspar, J. V.; Sullivan, B. P.; Kober, E. M.; Meyer, T. J.Application oft the Energy-gap Law to the Decay of Charge-transfer Excited States-Solvent Effects. *Chem. Phys. Lett.* **1982,** *91*, 91-95.

(5) Caspar, J. V.; Meyer, T. J. Photochemistry of $Ru(Bpy)_3^{2+}$-Solvent Effects. *J. Am. Chem. Soc.* **1983,** *105*, 5583-5590.

(6) Meyer, T. J. Photochemistry of Metal Coordination Complexes-Metal to Ligand Charge-Transfer Excited-States. *Pure and Appl. Chem.* **1986,** *58*, 1193-1206.

(7) Elias, H.; Chou, M. H.; Winkler, J. R. Electron-Transfer Kinetics of Zn-substituted Cytochrome *c* and Its $Ru(NH_3)_5$(Histidine-33) Derivative. *J. Am. Chem. Soc.* **1988,** *110*, 429-434.

(8) Tremain, S. M.; Kostic, N. M. Molten-globule and Other Conformational Forms of Zinc Cytochrome *c*. Effect of Partial and Comple Unfolding of the Protein on its Electron-transfer Reactivity. *Inorg. Chem.* **2002,** *41*, 3291-3301.

(9) Makarov, V.; Pettitt, B. M.; Feig, M. Solvation and Hydration of Proteins and Nucleic Acids: A Theoretical View of Simulation and Experiment. *Acc. Chem. Res.* **2002,** *35*, 376-384.

(10) Otting, G.; Liepinsh, E.; Wuthrich, K. Protein Hydration in Aqueous Solution. *Science* **1991,** *254*, 974-980.

(11) Denisov, V. P.; Halle, B. Hydration of Denatured and Molten Globule Proteins. *Faraday Discuss.* **1996,** *103*, 227-244.

(12) Zemel, H.; Hoffman, B. M. Long-range Triplet-triplet Energy Transfer Within Metal-substituted Hemoglobins. *J. Am. Chem. Soc.* **1981,** *103*, 1192-1201.

(13)   Soper, A. K.; Castner, E. W.; Luzar, A. Impact of Urea on Water Structure: a Clue to Its Properties as a Denaturant? *Biophys. Chem.* **2003,** *105*, 649-666.

(14)   Pace, C. N.; Laurents, D. V.; Thomson, J. A. pH Dependence of the Urea and Guanidine-hydrochloride Denaturation of Ribonuclease-A and Ribonuclease-T1. *Biochemistry* **2990,** *29*, 2564-2572.

(15)   Monera, O. D.; Kay, C. M.; Hodges, R.S. Protein Denaturation with Guanidine-hydrochloride or Urea Provides a Different Estimate of Stability Depending on the Contributions of Electrostatic Interactions. *Protein Science* **1994,** *3*, 1984-1991.

(16)   Ensign, A.A.; Jo, I.; Yildirim, I.; Krauss, T.D.; Bren, K.L. Zinc Porphyrin: A Fluorescent Acceptor in Studies of Zn-cytochrome *c* Unfolding by Fluorescence Resonance Energy Transfer. *Proc. Natl. Acad. Sci. USA* **2008,** *105*, 10779-10784.

(17)   Tokita, Y.; Shimura, J.; Nakajima, H.; Goto, Y.; Watanabe, Y. Mechanism of Intramolecular Electron Transfer in the Photoexcited Zn-substituted Cytochrome *c*: Theoretical and Experimental Perspective. *J. Am. Chem. Soc.* **2008,** *130*, 5302-5310.

(18)   Lee, J.C. Thesis, California Institute of Technology, 2002.

(19)   Mines, G.A. Thesis, California Institute of Technology, 1997.

(20)   Tezcan, F.A. Thesis, California Institute of Technology, 2001.

(21)   Pletneva, E.V.; Zhao, Z.Q.; Kimura, T.; et al. Probing the Cytochrorne *c'* Folding Landscape, *J. Inorg. Biochem.* **2007**, *101*, 1768-1775.

(22)   Pletneva, E.V.; Gray, H.B.; Winkler, J.R. Snapshots of Cytochrome *c* Folding. *Proc.Natl. Acad. Sci U.S.A.* **2005**, *102*, 18397-18402.

(23)   Pletneva, E.V.; Gray, H.B.; Winkler, J.R. Many Faces of the Unfolded State: Conformational Heterogeneity in Denatured Yeast Cytochrome *c*. *J. Mol. Bio*. **2005**, *345*, 855-867.

(24)   Lyubovitsky, J.G.; Gray, H.B.; Winkler, J.R. Structural Features of the Cytochrome *c* Molten Globule Revealed by Fluorescence Energy Transfer Kinetics. *J. Am. Chem. Soc*. **2002**, *124*, 14840-14841.

(25)   Lyubovitsky, J.G.; Gray, H.B.; Winkler, J.R. Mapping the Cytochrome *c* Folding Landscape. *J. Am. Chem. Soc.* **2002**, *124*, 5481-5485.

(26)   Lyubovitsky, J.G.; Winkler, J.R.; Gray, H.B. Real-time Folding Dynamics of S-cerevisiae iso-1 Cytochrome *c*. *J. Inorg. Biochem.* **2001**, *86*, 322-322.

(27)   Kimura, T.; Lee, J.C.; Gray, H.B.; et al. Folding Energy Landscape of Cytochrome cb(562). *Proc.Natl. Acad. Sci U.S.A.* **2009**, *106*, 7834-7839.

(28)   Kimura, T.; Lee, J.C.; Gray, H.B.; et al. Site-specific Collapse Dynamics Guide the Formation of the Cytochrome *c'* Four-helix Bundle. *Proc.Natl. Acad. Sci U.S.A.* **2007**, *104*, 117-122.

(29)   Lee, J.C.; Engman, K.C.; Tezcan, F.A.; et al. Structural Features of Cytochrome *c'* Folding Intermediates Revealed by Fluorescence Energy-transfer Kinetics. *Proc.Natl. Acad. Sci U.S.A.* **2002**, *99*, 14778-14782.

(30)   Faraone-Mennella, J.; Tezcan, F.A.; Gray, H.B.; et al. Stability and Folding Kinetics of Structurally Characterized Cytochrome c-b(562). *Biochemistry* **2006**, *45*, 10504-10511.